ELSEVIER

Journal of Nuclear Materials 250 (1997) 171–175

journal of nuclear materials

Reactions between U–Zr alloys and Fe at 923 K

Takanari Ogata [a,*], Masaki Kurata [a], Kinya Nakamura [a], Akinori Itoh [b], Mitsuo Akabori [b]

[a] *Central Research Institute of Electric Power Industry, Iwato-kita 2-11-1, Komae-shi, Tokyo 201, Japan*
[b] *Japan Atomic Energy Research Institute, Tokai-mura, Ibaraki-ken 319-11, Japan*

Received 2 April 1997; accepted 3 August 1997

Abstract

Interdiffusion experiments were carried out at 923 K with the diffusion couples consisting of U–23 at.% Zr/Fe and U–23 at.% Zr–1 at.% Ce/Fe. The reaction layer adjacent to the Fe was a single Zr-depleted UFe_2 phase. The phases in the reaction layers were estimated consistently with the calculated U–Zr–Fe ternary isotherm. The diffusion path obtained in this study was similar to that reported for the U–Pu–Zr/HT9-steel couple at 923 K, when those paths were expressed on the (U + Pu)–Zr–(Fe + Cr) composition triangle. The reaction layers grew in proportion to the square root of the annealing time. The addition of approximately 1 at.% of Ce to the U–23 at.% Zr alloy has little effect on the reaction between U–23 at.% Zr and Fe. © 1997 Elsevier Science B.V.

PACS: 66.30.Ny; 28.41.Bm; 68.35.Fx

1. Introduction

Uranium–plutonium–zirconium (U–Pu–Zr) alloys have been recognized as good alternatives for the advanced fast reactor fuel because of their high burnup capability and favorable thermal response. During the use of these metallic fuel pins in a reactor, however, metallurgical reactions occur between the fuel alloys and the cladding materials [1]. The reaction layers formed include phases with liquefaction temperatures below 950 K. For example, the liquid phase formation at the fuel–cladding interface was observed in the irradiated fuel pin segment (U–19 wt% Pu–10 wt% Zr alloy clad with HT9 [1]) after out-of-pile annealing at 933 K [2]. Since the fuel matrix liquefaction during the steady state is not acceptable, the peak cladding inner temperature should be designed to be lower than the liquid phase formation temperature. This threshold value has not yet been determined.

In order to evaluate the liquid phase formation temperature, it is required (1) to clarify compositions and structures of the reaction layers formed between the fuel alloys and the cladding materials and then (2) to identify the critical phase in the reaction layers and its liquefaction temperature. With respect to (1), several ex-reactor experiments have been carried out with various diffusion couples consisting of the fuel alloys and Fe-base alloys [3] and the fuel alloys and the cladding materials [4–6].

The present study investigates the compositions and structures of the solid-state reaction layers formed at 923 K at two kinds of diffusion interfaces: U–23 at.% Zr/Fe and U–23 at.% Zr–1 at.% Ce/Fe. Ce is a stand-in for the rare earth fission products. An estimation of the phases in the reaction layers is presented in this report. The result is compared with the previous study on the couple of the U–Pu–Zr alloy and HT9 [5,6]. The investigation on this kind of simpler system is expected to serve as a theoretical

* Corresponding author. Tel.: +81-3 3480 2111; fax: +81-3 3480 7956; e-mail: pogata@criepi.denken.or.jp.

[1] HT9 is a stainless steel with the following composition in wt%: Cr, 12; Mo, 1; Ni, 0.5; W, 0.5; V, 0.3; Si, 0.25; Mn, 0.2; C, 0.2; Fe, bal.

PII S0022-3115(97)00262-6

basis for the analysis of the fuel-cladding metallurgical reaction.

2. Experimental procedure

The U–Zr and U–Zr–Ce alloy specimens used in this study were prepared from the pure U, Zr and Ce metals by arc-melting in a highly purified argon atmosphere on a water-cooled copper hearth. Compositions of the arc-melted ingots are summarized in Table 1. Both of the ingots were wrapped in a tantalum foil, encapsulated in a quartz tube under an atmosphere of 0.025 MPa helium and then homogenized at 1123 K for 48 h. Cerium precipitates were observed in the U–Zr–Ce alloy, which indicated that the alloy matrix was saturated with Ce. The homogenized ingots and the Fe plate of 99.995% purity were cut into blocks with a size of $4 \times 4 \times 2$–3 mm. The Fe block was sandwiched between the U–Zr and U–Zr–Ce blocks to form a diffusion couple, as shown in Fig. 1. The block surfaces which act as interfaces of the diffusion couple were polished with 3 μm diamond paste. To clarify the initial interface position, Ta foil of 10 μm thickness with a window of 2×2 mm size was inserted into the interfaces. Three diffusion couples were made, each of which was encapsulated in the 316 stainless steel holder. Tantalum foils were placed inside the holder to prevent the couple from reacting with the stainless steel. Each of the diffusion couple assemblies was encapsulated in a quartz tube under an atmosphere of 0.025 MPa helium.

The three diffusion couples were annealed isothermally at 923 K for 256, 407 and 832 h, respectively. After completion of the diffusion anneal, the couples were quenched in water, then sectioned parallel to the diffusion direction. The sectioned couple was embedded in epoxy resin and then the cross-sectional surface was polished with 3 μm diamond paste for the electron probe microanalysis (EPMA). Concentration distributions of U, Zr, Fe and Ce in the diffusion zone were measured by an electron probe microanalyzer (Simadzu Co. EPM-810, wave length dispersive) operated at 25 kV. The intensities of the U–Mα, Zr–Lα, Fe–Kα and Ce–Lα X-rays were converted to atomic fractions by using the ZAF correction. The reaction layer thickness was measured on the back-scattered electron image.

3. Results

3.1. Structures of reaction layers

Fig. 2 shows the back-scattered electron images of the reaction zone at the U–Zr/Fe interface after annealing at 923 K for 407 h. Black spots in the images are Zr-rich precipitates, presumably combined with oxygen or nitrogen impurities. The reaction zone can be divided into six layers as indicated in Fig. 2. The Ta foils inserted into the initial interfaces were observed on the Fe side in layer D, which indicates that a larger reaction layer was formed on the U–Zr side than on the Fe side. These reaction layer structures were independent of the annealing time and the existence of Ce. Such a Ce-enriched zone was not found in the U–Zr–Ce/Fe interfaces. From Fig. 2, layer A seems to be a single phase, while layers B, D and E have two-phase structures. Layer C was very thin and seems to be a single phase. Layer F appears to include a slightly brighter phase.

The quantitative EPMA result indicated that the single phase layer A was UFe_2 and included a negligible amount of Zr. Since the phases in the other layers were too minute to determine the compositions quantitatively, the averaged compositions of each of these layers were obtained in the following manner. The sample stage in the microanalyzer was moved to the diffusion direction with 2–10 μm intervals, then the local compositions measured were averaged over each of these layers. The average compositions thus obtained for the layers D, E and F are plotted on the U–Zr–Fe composition triangle (Fig. 3), where Ce contents are ignored.

The U–Zr–Fe ternary isotherm at 923 K (Fig. 4) [7] was calculated to identify the phases in the reaction layers. When calculating Fig. 4, the following were assumed: (a) immiscibility between UFe_2 and $ZrFe_2$ and (b) the formation of the ternary intermediate phases, ε and λ, which were observed in the preliminary metallography for the U–Zr–Fe alloy samples [8]. By comparing Fig. 3 with Fig. 4, it can be estimated that layers D, E and F are two-phase layers, $U_6Fe + ZrFe_2$, $U_6Fe + \varepsilon$ and $\alpha U + \lambda$, respectively. Although Fig. 4 suggests the formation of the two-phase layer, $\alpha U + \varepsilon$, the present methodology could not distinguish it from $U_6Fe + \varepsilon$.

Table 1
Compositions of the arc-melted ingots

Name	U (g)	Zr (g)	Ce (g)	U (at.%)	Zr (at.%)	Ce (at.%)
U–23 at.% Zr	34.213	4.112	–	76.13	23.88	–
U–23 at.% Zr–1 at.% Ce	34.502	4.118	0.356	75.25	23.44	1.32

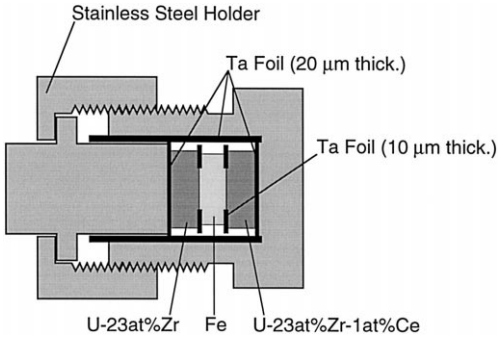

Fig. 1. Schematic view of the diffusion couple assembly.

The compositions of the thin layers B and C are estimated from the phases of the adjacent layers and the contrasts of Fig. 2; B is a two-phase layer of $UFe_2 + U_6Fe$ and C is a single $ZrFe_2$ phase layer. The diffusion path for the U–23 at.% Zr/Fe couple at 923 K can be drawn by connecting the layer compositions, as shown by the dotted line in Fig. 4.

3.2. Growth of reaction layers

Fig. 5 shows plots of thicknesses of the layers versus the square root of the annealing time, t. As the boundary between layers D and E was rather ambiguous, the sum of these thicknesses is plotted. The sum of layer A and B thicknesses is also plotted for the same reason. Fig. 5 shows the reaction layer thicknesses grow in proportion to $t^{1/2}$. This confirms that the reaction is diffusion-controlled.

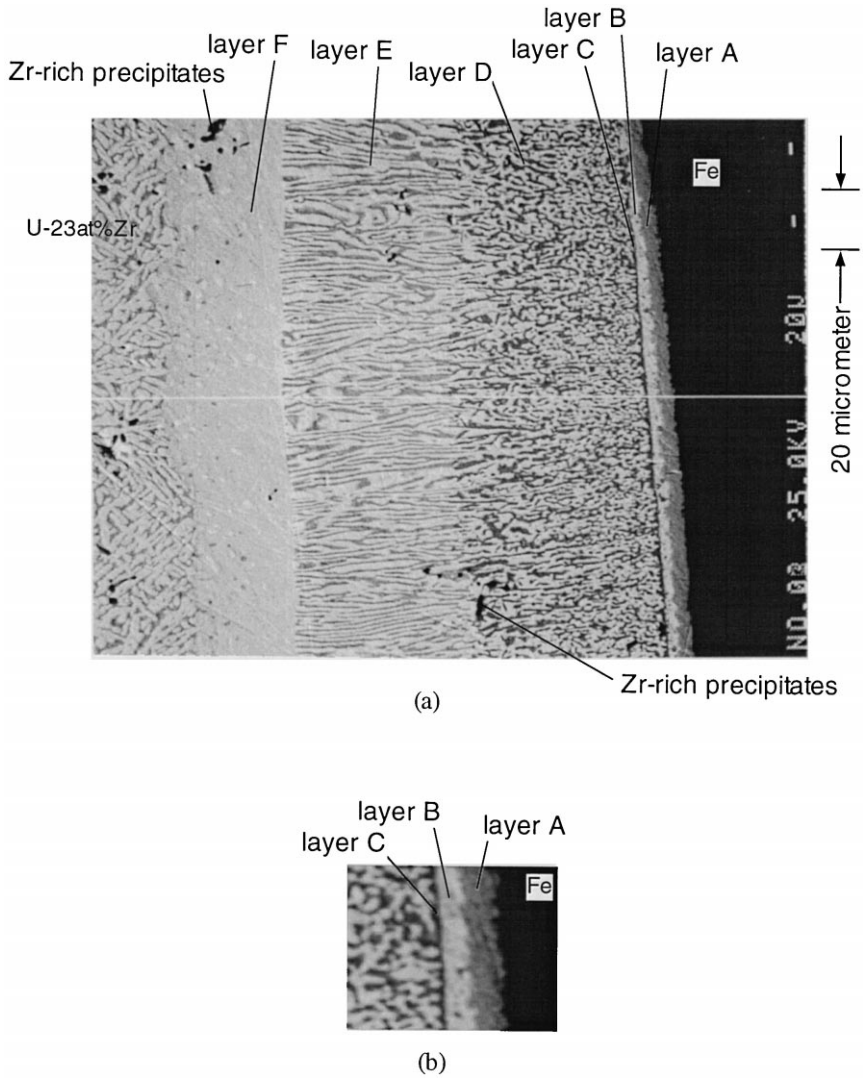

Fig. 2. Back-scattered electron image of U–23 at.% Zr/Fe interface after annealing at 923 K for 407 h: (a) and (b) are at two different magnifications.

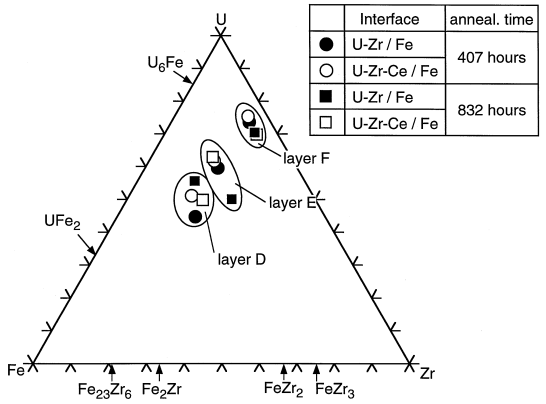

Fig. 3. Average compositions of the reaction layers D, E and F.

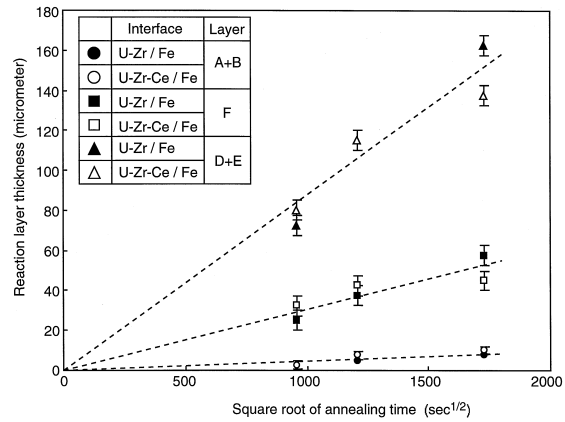

Fig. 5. Growth of the reaction layers.

The effect of Ce on the reaction layer growth can not be found in Fig. 5.

4. Discussion

4.1. Relation with the Pu-containing system

Keiser and Petri [5,6] examined the diffusion structure of the U–22 at.% Pu–23 at.% Zr/HT9 couple annealed at 923 K for 100 h. They found the following diffusion layers on the HT9 toward the U–Pu–Zr side as shown in Fig. 6: a single-phase layer (U, Pu, Zr)(Fe, Cr)$_2$, a two-phase (U, Pu, Zr)$_6$(Fe, Cr) + (U, Pu, Zr)(Fe, Cr)$_2$, a single-phase (Zr, U, Pu)(Fe, Cr)$_2$ and a two-phase (Zr, U, Pu)(Fe, Cr)$_2$ + (U, Pu, Zr)$_6$(Fe, Cr). These layers are similar to those estimated in the present study for the U–Zr(–Ce)/Fe couples: a single-phase layer UFe_2 (layer A), a two-phase U_6Fe + UFe_2 (layer B), a single-phase $ZrFe_2$ (layer C) and a two-phase $ZrFe_2$ + U_6Fe (layer D), respectively. This similarity can be also illustrated by comparison of the diffusion path for the U–Zr(–Ce)/Fe couple drawn on the U–Zr–Fe triangle (Fig. 4) with that for the U–Pu–Zr/HT9 on the (U + Pu)–(Fe + Cr)–Zr triangle (Fig. 6). It can be stated that the present test result for the simple U–Zr(–Ce)/Fe couples serves for the basis of the analysis for the reaction between the U–Pu–Zr fuel and the stainless steel cladding.

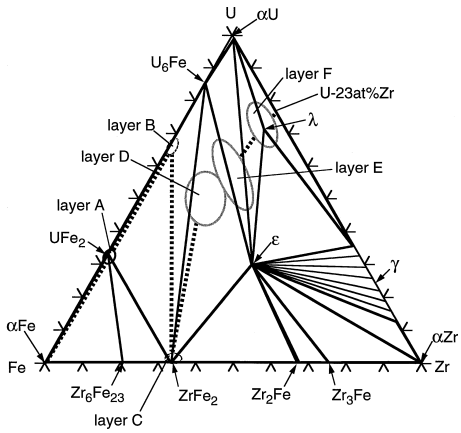

Fig. 4. The U–Zr–Fe ternary isotherm evaluated at 923 K [7], assuming no solid solution between UFe_2 and Fe_2Zr and formation of the ternary compounds, ε and λ. The grey circles show data bands of average compositions of the reaction layers D, E, F. Dotted lines show the estimated diffusion path.

4.2. Behavior of Ce

In the post-irradiation examinations of the metallic fuel pins, the phase rich in rare earth fission products was observed in the reaction zone in the cladding [1]. However, no Ce-rich phase was detected in the present test. This suggests that the enrichment of rare earth elements is not produced only by an isothermal diffusion mechanism.

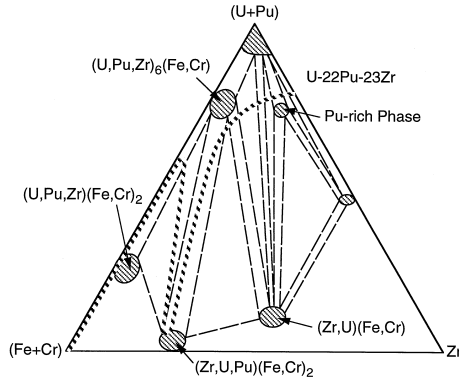

Fig. 6. An experimental diffusion path (dotted bold lines) on a composition triangle at 923 K for the U–22 at.% Pu–23 at.% Zr versus HT9 couple [5], reproduced with permission.

5. Conclusion

Interdiffusion experiments were carried out at 923 K with the diffusion couples consisting of U–23 at.% Zr/Fe and U–23 at.% Zr–1 at.% Ce/Fe. The reaction layer adjacent to the Fe was a single Zr-depleted UFe_2 phase. The phases in the reaction layers were estimated consistently with the calculated U–Zr–Fe ternary isotherm. The diffusion path obtained in this study was similar to that reported for the U–Pu–Zr/HT9-steel couple at 923 K, when those paths were expressed on the (U + Pu)–Zr–(Fe + Cr) composition triangle. The reaction layers grew in proportion to the square root of the annealing time. The addition of approximately 1 at.% of Ce to the U–23 at.% Zr alloy had little effect on the reaction between U–23 at.% Zr and Fe.

Acknowledgements

The authors appreciate valuable discussions with Dr T. Ogawa of Japan Atomic Energy Research Institute and Mr T. Yokoo of Central Research Institute of Electric Power Industry. We also wish to thank Dr D.D. Keiser Jr. of Argonne National Laboratory-West for permission to reproduce fig. 3 of Ref. [5].

References

[1] B.R.T. Frost, ed., Materials Science and Technology: A Comprehensive Treatment, Nuclear Materials, Vol. 10A (VCH, New York, 1994).
[2] A.B. Cohen, H. Tsai, L.A. Neimark, J. Nucl. Mater. 204 (1993) 244.
[3] D.D. Keiser Jr., M.A. Dayananda, J. Nucl. Mater. 200 (1993) 229.
[4] D.D. Keiser Jr., M.A. Dayananda, Metall. Mater. Trans. 25A (1994) 1649.
[5] D.D. Keiser Jr., M.C. Petri, Proc. 15th Ann. Conf. of the Can. Nucl. Soc., Montreal, Canada, June 5–8, 1994, p. 5C.
[6] D.D. Keiser Jr., M.C. Petri, J. Nucl. Mater. 240 (1996) 51.
[7] M. Kurata, T. Ogata, K. Nakamura, T. Ogawa, to be published.
[8] K. Nakamura, M. Akabori, A. Itoh, unpublished work.